SciEn

Proceedings of 8th International Conference on Mechanical, Industrial and Energy Engineering 2024
02-04 January, 2025, Khulna, BANGLADESH

SciEn Conference Series: Engineering Vol. 3, 2025, pp 370-376 https://doi.org/10.38032/scse.2025.3.103

Enhancement of Aerodynamic Performance of NACA 4415 2D by Adjoint Optimization and Vortex Generators using CFD Analysis

Md Saifur Rahman[1,], Khairun Nasrin Rimi[2], Md Mahir Shahriar[1]*

[1]Department of Mechanical Engineering, Chittagong University of Engineering & Technology, Chattogram, Bangladesh
[2]Department of Mechanical Engineering, Bangladesh University of Engineering and Technology, Dhaka, Bangladesh

ABSTRACT

This study presents a comprehensive computational fluid dynamics (CFD) analysis of the NACA 4415 airfoil utilizing the k-omega SST (Shear Stress Transport) turbulence model. The airfoil's aerodynamic parameters such as lift, drag, and pressure distribution are analyzed under various flow conditions corresponding to Reynolds numbers. The preliminary focus is to investigate airfoil performance on different angle of attack over a range of Reynolds numbers from 200,000 to 500,000. Additionally, the aerodynamic effects of vortex generators on the airfoil performance have been analyzed. Three different shapes vortex generators, positioned 100mm distance from the airfoil tip, are used to analyze the performance. Additionally, adjoint optimization techniques enhance the airfoil's aerodynamic characteristics. On the adjoint optimization the airfoil lift to drag ratio is increased by 5-10% compared to the base case. The CFD simulations are conducted using ANSYS Fluent software, using the k-omega SST turbulence model as its accuracy to capture turbulent flows with separation. Lift to drag ratios for airfoil with vortex generator are comparatively less than the base case lift to drag ratio of 18.5075. Lift to drag ratio of airfoil with vortex generator in 0° to 25° degree varies from 1 to 25. For Adjoint optimization of the airfoil, three trials are taken and two found satisfactory compared to the base airfoil. Lift to drag ratio is increased by 18% to 20% from the base airfoil for first two cases. But further increase resulted more drag in the airfoil, trial three lift to drag ratio decreased to 15, representing an 18% reduction in lift to drag ratio and 45% increase in drag. The results offer valuable insights for designing and optimizing airfoils in aerospace and other high-Reynolds-number applications.

Keywords: K-omega SST model, Vortex generator, Lift to drag ratio, Adjoint optimization, Aerodynamic analysis

1. Introduction

Wind power, one of several renewable energy sources, has grown dramatically in recent years. Wind energy prices are not competitive when compared to fossil energy prices, and this is due to the establishment of energy pricing policies through subsidies[1]. Before building the Wind Energy Conversion System, computational fluid dynamics simulations must be performed to save design time and cost. The NACA 4415 airfoil is the most commonly utilized aerodynamic form in wind turbine blade applications[2].

The ground effect of three types of airfoils, NACA 0015, NACA 4415, and NACA 6415, in a low-speed wind tunnel was studied by Ahmed [3]. To determine the minimum ground clearance for different chord lengths experiments were done at angles of attack ranging from 0° to 100°. Results indicate that high pressure under the airfoil surface corresponds with coefficient values closer to the ground. High average speeds are shown around peak locations of The NACA 4415 model. The control of the boundary layer is an important issue in the field of aerodynamics that determines the lift and drag loss of the fluid mechanics, so improving the control of boundary layer problems is an essential field of study[4]. The use of flow control and control methods on airfoils is vital. There are numerous studies on flow control methods. As a result, numerous flow control research studies[5]–[7] can be reviewed for more information. Flow control technologies are roughly characterized as active or passive[8]. It is active when applied with external energy. Passive methods control the flow without the use of external power. Dielectric barrier discharge (DBD) plasma actuators[8], blowing[9], and suction are examples of active approaches. Passive approaches typically affect the shape. Passive approaches include gurney flaps[10], roughness[11], [12], dimples[13], adding cavities or bumps to the airfoil[14]–[16], modifying the geometry of the leading edge, and employing vortex generators.

Vortex generators (VGs) are the most common and effective devices[17], [18], with a wide range of technical applications, but they are mostly utilized in flow separation, control, mixing, and heat transfer[19]. Conventional VGs should have a height h equal to the thickness of the boundary layer (δ) for optimal performance across a wide range of flow conditions[17], [18]. Vortex generators can excite local instability waves, causing an early shift to turbulence. This delays flow separation and reduces the separation zone size[20]. Angele et al. [21] investigated the use of streamwise vortices from a VG to regulate a separating boundary layer. The counter-rotating vortices from one VG drifted apart in the spanwin zone.

Extensive research on riblets, which are micro-grooves aligned with the freestream direction, has yielded encouraging results[22], [23]. In recent years, we have reached flight trails. Previous studies using riblets with symmetric v-grooves (height equal to spacing) and 3M adhesive-backed film (USA) demonstrated great consistency in lowering drag and enhancing flow structure[22]. Riblets have been proven to lower viscous drag by 4-8% in two-

*Corresponding Author Email Address: mdsaifur.rahman.me@gmail.com PublishedBy: SciEn Publishing Group

dimensional flows with no or minimal pressure gradients. These findings have stimulated research into their applicability at transonic speeds and in flight. Wall shear stress rises near groove peaks but falls in the valley[24], [25], resulting in a net drag reduction despite the increased wetted surface.

An adjoint system requires a numerical study of its underlying equations. The adjoint equations are not directly derived from a physical model and require a different numerical approach than the fluid equations. Stability and convergence should be examined independently. The discrete adjoint formulation involves discretizing and differentiating the flow equations[26]–[28]. The governing equations are three-dimensional Reynolds averaged Navier-Stokes equations discretized in space with a cell-centered finite-volume formulation on structured multiblock grids[29]. The continuous adjoint approach for calculating shape sensitivity in aeronautical design using turbulence modeling is explained and developed by Bueno-Orovio et al. [30]. The study focuses on compressible flows using the Reynolds-averaged Navier-Stokes equations and the classical Spalart-Allmaras turbulence model. Turbulence modeling usually needs the determination of the distance to the surface.

For this study of NACA4415, a base airfoil is set and numerical analysis conducted on different Angle of Attack. Then analyzing the results of numerical analysis, the airfoil is being introduced to vortex generator and continuous Adjoint optimization to optimize its aerodynamics. Thus, it results in increment in lift and lift to drag ratio.

2. Numerical Modeling

2.1 Computational Domain

A C-type domain is set for the airfoil numerical analysis. Because it effectively represents the boundary layer behavior and wake flow in high-resolution regions close to the airfoil surface, the C-type domain grid is frequently utilized in airfoil CFD simulations. C is the chord length of the airfoil where C=1m. Domain size and shape are carefully considered as they play a crucial role in the accuracy and reliability of the computational outcomes.

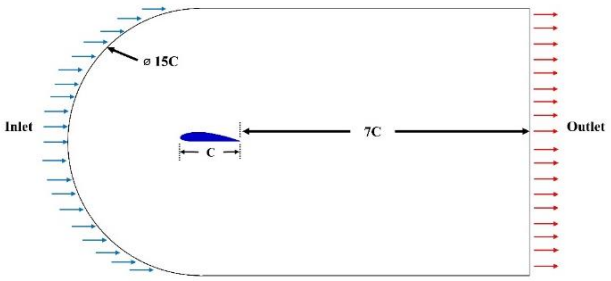

Figure 1: Fluid domain NACA4415 airfoil (C=1m)

The fluid domain used for computational analysis is shown in Figure 2. This graphic representation offers a thorough picture of the area that the computational simulation is examining.

2.2 Mesh and Grid Independent Test

For the computational analysis of NACA4415, the computational domain is meshed. The mesh is made of quadrilaterals throughout the entire computational domain. The mesh type used in this study is Quadrilateral Dominant. To capture the intricate details of the flow field around the airfoil, the mesh close to the airfoil made dense. The node-to-node distance near airfoil starts from 0.004914mm gradually increase to 0.039002 in the far field. Intricate mesh near the airfoil boundary allows the results to be more accurate. The distance from the wall to the first grid point or the Y+ value of the airfoil is set to 0.005.

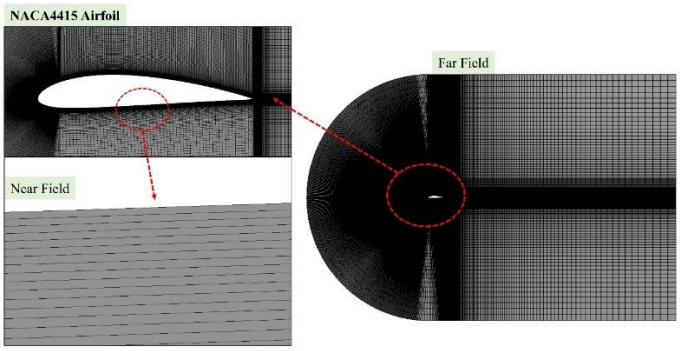

Figure: Mesh setup of NACA4415

The figure shows the meshing of NACA4415 airfoil computational domain after fine meshing with nodes of 1201196 and elements of 1198400.

A Grid Independent Test is conducted for the simulation setup where mesh size varied from coarse to fine. An initial mesh setup with 79100 no's elements and fine mesh with 7030730 no's elements. As the mesh gets finer the results became more stable and converged on a liner pattern.

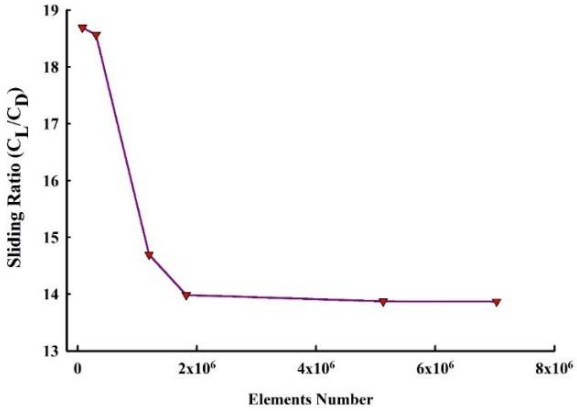

Figure 2: Grid Independent Test of NACA4415

2.3 Governing equations and boundary conditions

The pressure-based solver with a constant density was used to simulate in a steady-state manner. For this investigation, ANSYS 2020 R1 is utilized. The k-omega SST turbulence model was selected for the simulation. The output static gauge pressure was set to zero, and the velocity at the domain's inlet ranged from 3 to 7 meters per second. The airfoil and the fluid domain walls are subject to the no-slip condition.

2.3.1 Numerical scheme

The intensity and length scale approach were used to take wind velocity variations into consideration. In particular, 7% of the characteristic length, or roughly 0.07 m, was subjected to a turbulence intensity of 0.25%. At 25 ° C ambient temperature, air has a density of approximately 1.184 kg/m³

and a viscosity of about 1.846×10^{-5} Pas is maintained while conducting the airfoil analysis. Second-order discretization and the Semi-Implicit Method for Pressure Linked Equations (SIMPLE) technique for pressure-velocity coupling were used to solve the Reynolds-Average Navier-Stokes (RANS) equations. The simulation was iterated until convergence, attaining root mean square residual values of 10^{-12}, with care given to ensure the numerical values were correct.

2.3.1.1 Mathematical Modeling

The external flow condition of the airfoil is simulated by solving the Navier-Stokes equations, which govern the preservation of mass, momentum, and energy in fluid flow. The following is a mathematical expression for these equations:

a. Continuity Equation:

The continuity equation, which expresses the conservation of mass, is given by:

$$\frac{\partial u}{\partial x_l}(\rho x_l) = 0 \tag{2.1}$$

where ρ is the density of the fluid and u is the velocity vector.

b. Navier-Stokes Equations:

The following are the Navier-Stokes equations, which explain the conservation of momentum:

$$\rho\left(\frac{\partial u}{\partial t} + u\frac{\partial u}{\partial x_l}\right) = -\frac{\partial u}{\partial x_l}P + \mu\left(\frac{\partial u}{\partial x_l}\right)^{2u} + \rho g \tag{2.2}$$

where P is the pressure, μ is the dynamic viscosity of the fluid, and g is the gravitational acceleration.

For calculation the Coefficient of drag (Cd):

$$C_d = \frac{2F_d}{\rho v^2 A} \tag{2.3}$$

Here F_d is the drag force, ρ is the density of fluid, V is the velocity of fluid and A is the reference area.

In CFD, the Y+ value is an important parameter for determining the accuracy of the boundary layer thickness. Mathematically, the Y+ value can be calculated as:

$$Y + \frac{u\tau \times y}{\mu} \tag{2.4}$$

Here, u_τ is the friction velocity, y is the wall distance, and μ is the kinematic viscosity of the fluid.

2.3.2 Adjoint Optimization

Adjacent optimization is a potential tool when developing and constructing aerodynamic designs, such as wind turbine blades, automobile bodywork, or aviation wings[31]. It combines techniques from computational fluid dynamics (CFD), optimization algorithms, and the adjoint approach.

2.3.2.1 Adjoint Equations

The adjoint technique is an efficient method to calculate the gradients of an objective function with respect to design factors. The objective function typically relates to aerodynamic performance, such as enhancing lift or decreasing drag. The design variables are elements that can be altered to modify the geometry, like wing twist or airfoil thickness. In the earlier work, the following mathematical formulations were mentioned[32]:

$$R^p = -\frac{\partial v_i}{\partial x_i} = 0 \tag{6}$$

$$R_i^v = v_j\frac{\partial v_i}{\partial x_i} + \frac{\partial p}{\partial x_j} - \frac{\partial}{\partial x_j}\left[(v + v_t)\left(\frac{\partial v_i}{\partial x_j} + \frac{\partial v_j}{\partial x_i}\right)\right] = 0 \tag{7}$$

$$R_i^z = Convection + Diffusion + Production + Disipation = 0 \tag{8}$$

Primal velocity is denoted by v_i, primal pressure by p, and turbulent kinematic viscosity by v and v_t. Again, the surface and volume integrals for the objective function F are:

$$F = \int_S F_s dS + \int_S F_\Omega d\Omega \tag{9}$$

$$F_{aug} = F + \int_\Omega qR^p d\Omega + \int_\Omega u_i R_i^v d\Omega \tag{10}$$

The adjoint variables, q and u_i, can be read as "adjoint pressure" and "adjoint velocity," respectively, depending on how they enter the solution process. The following formula can be used to determine the surface sensitivity of the objective function with regard to the surface normal motion of the surface nodes (design variables) once the adjoint equations have been solved:

$$\frac{\delta F_{aug}}{\delta b} = -\int_{S_w}\left[(v + v_t)\left(\frac{\partial v_i}{\partial x_j} + \frac{\partial v_j}{\partial x_i}\right) - qn_i\right]\frac{\partial v_j}{\partial x_k}\frac{\partial x_k}{\partial b_m}\,dS \tag{11}$$

Furthermore, the adjoint far-field boundary condition just specifies that free stream conditions are applicable there and the far-field's geometrical position is fixed. The concept of "adjoint optimization" involves calculating a function's derivative with respect to the parameters of interest and then adjusting the parameters to optimize the function. Figure 3 displays a schematic diagram of the adjoint approach utilized in this investigation.

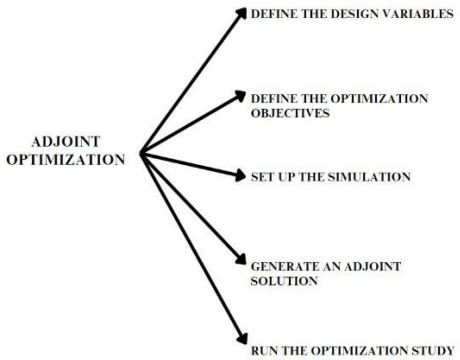

Figure 3: Adjoint optimization approach and steps

Establishing the boundary to run the adjoint solver and determining the airfoil's lift to drag ratio are the first steps in the study. To get the intended results, a number of parameters are then adjusted in the Ansys solver settings, including observable lift, observable drag, percentage increment, pressure solver, etc. The important observable is the lift to drag ratio, which measures an aerodynamic design's efficiency. Its value is increased by a percentage increment. Additionally, the gradient is based on the least squares cell and the adjoint solution approach is applied. A second-order approach was used to calculate the pressure, guaranteeing

accurate pressure distribution in the results. Additionally, 1,000 iterations are used with convergence criteria set to 1×10^{-12}, which can further challenge achieving optimal designs if the solution remains sensitive to initial conditions or boundary definitions.

2.3.2.1 Adjoint Analysis Domain

For adjoint analysis of the NACA4415 airfoil, a smaller boundary region is captured of 2m length and 1.5m of width shown in figure. This small region encompassing the airfoil shape is analyzed for optimization of the airfoil. With the increase in the lift to drag ratio, the sensitivity of this region will change; thus, the airfoil shape will also be altered.

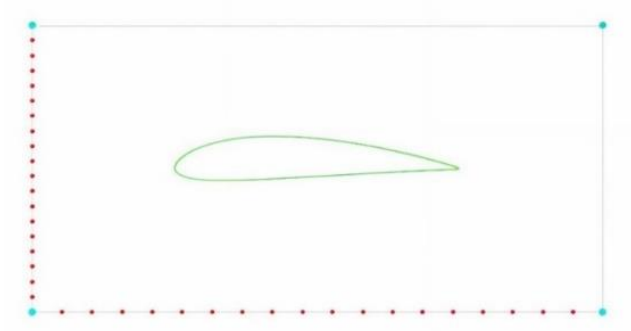

Figure 4: Adjoint Optimization close domain

Adjoint optimization region geometry defines the area used to assess the sensitivity of the objective function to optimization parameters. It includes the boundary where flow interacts with the solid body, requiring velocity and pressure computations to evaluate drag and sensitivity to airfoil geometry changes. This region is determined using adjoint variables linked to the objective function and its derivatives.

2.4 Vortex Generator (VG)

For the analysis of NACA4415 airfoil, vortex generator of different shapes is used. In figure the vortex generator dimensions are depicted and its distance from the tip of the airfoil is denoted as D. For all vortex generator the distance kept constant on 100m shown in *Table 1*.

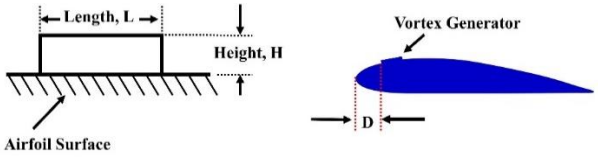

Figure 5: Vortex generator on airfoil

Vortex generator shapes are varied dimension from 100mm distance from the tip of the airfoil as marked in the picture.

Table 1: Vortex Generator Specifications

VG Case	Height, H (mm)	Length, L (mm)	Distance from Tip, D(mm)
1	5	50	100
2	8	75	100
3	10	100	100

3. Validation

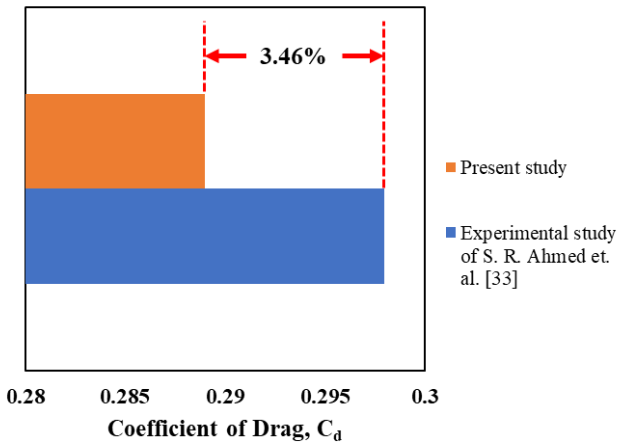

Figure 6: Comparative analysis of experimental study of S.R. Ahmed and the Ahmed body study

The present study's drag coefficient (0.289) closely matches the experimental result by S. R. Ahmed et al. [33] (0.298), validating the accuracy of the methodology.

4. Result and Discussion

4.1 Computational Analysis

NACA 4415 analyzed for four velocities varying Reynolds number within the range of 200000 to 500000 with air velocity varying from 3 to 7.5 ms^{-1}.

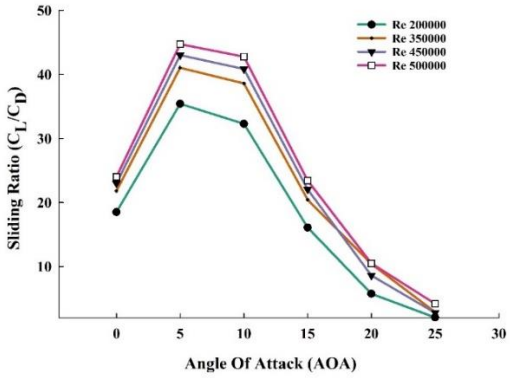

Figure 7: Naca 4415 lift to drag ratio change with difference Angle of Attack

For the airfoil Angle of Attack (AOA) changed from 0 to 25 with 5-degree difference. While analyzing the airfoil with varying angle of attached maximum lift to drag ratio is seen on 5 degrees of angle of attack and lift to drag ratio decreases with the increase in AOA. After conducting the computational analysis of airfoil on four Reynolds number 200000,350000,450000 and 500000. On 200000 Reynolds Number, the lift coefficient (Cl) climbs with increasing AOA; it peaks at 15 degrees, at 1.2235, and then starts to decline at higher angles. Additionally, there is a rising trend in the drag coefficient (Cd), which is especially noticeable at 25 degrees when it hits 0.3316, demonstrating that higher AOA is related with increased drag. since of this, the lift-to-drag ratio (Cl/Cd) shows a decrease, peaking at 35.4352 at 5 degrees and falling to 2.0545 at 25 degrees. This indicates

that although lift is increased at some angles, too much angle of attack (AOA) reduces aerodynamic efficiency since it increases drag. The significance of adjusting the AOA to attain a balance between lift and drag for enhanced airfoil design performance is shown by this analysis.

4.2 Vortex Generator (VG)

Three different shape vortex generators (VG) mentioned in *Table 1* are used to analyze their performance and impact with the NACA4415. These VGs are analyzed on Reynold Number 200000 in between 0° to 25° with a 5°Degree gradual increment in the AOA.

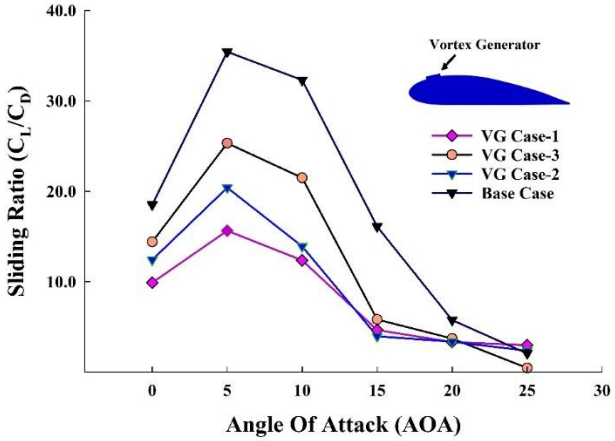

Figure 8: NACA 4415 Vortex Generator lift to drag ratio change with AOA

In Case-1, the lift coefficient (Cl) peaks at 10 degrees with a value of 0.9163. In contrast, the drag coefficient (Cd) increases significantly at higher angles, resulting in a declining lift-to-drag ratio (Cl/Cd). Case 2 shows a similar trend, with a maximum Cl of 0.9994 at 10 degrees, but it has a notably higher lift to drag ratio of 25.3260 at 5 degrees compared to the other cases. However, at 25 degrees, Case-2 experiences a significant drop in Cl to 0.3483 and an increase in Cd to 0.7749, resulting in a much lower lift to drag ratio of 0.4494. Case-3 generally maintains moderate performance with a peak Cl of 0.8124 at 10 degrees, but like the others, it suffers from increased drag at higher AOA, leading to lower aerodynamic efficiency.

Figure 10 shows the contour of NACA4415 with VG. VG's lift to drag ratio is less than the base airfoil lift to drag ratio. As AOA changes, the lift to drag ratio initially increases and decreases with higher AOA. A higher angle of attack creates a vortex behind the airfoil, which creates drag. Higher AOA creates drag, and the lift to drag ratio decreases as a result.

4.3 Adjoint Optimization

NACA4415 airfoil optimization is done using adjoint optimization. For optimization purpose, lift to drag ratio is set as observable and calculated to increase the value of lift to drag ratio. While optimizing the adjoint optimization on the airfoil, each adjoint calculation was run as trial.

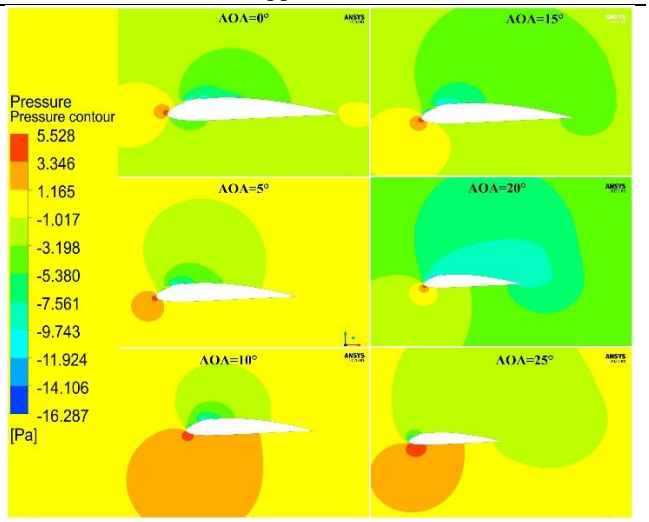

Figure 9: Pressure contour of NACA4415 with VG at different AOA

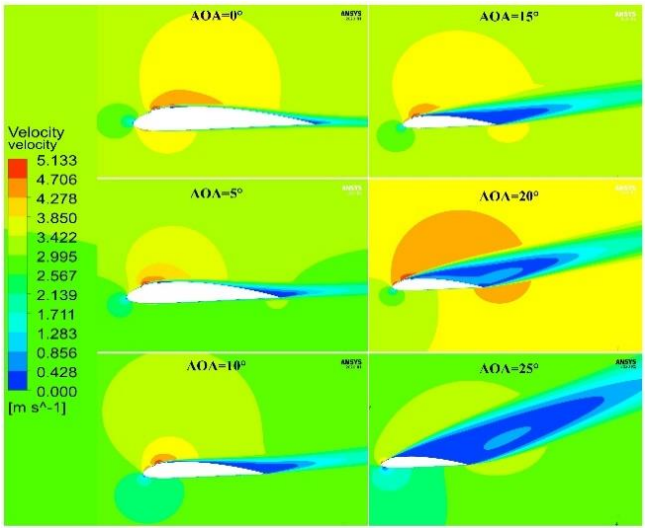

Figure 10: Velocity Contour of NACA4415 with VG at different AOA

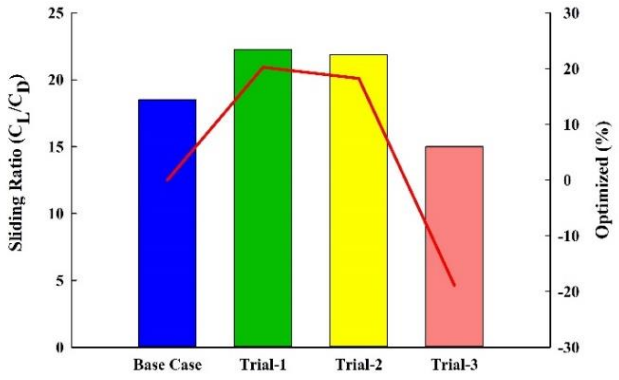

Figure 11: NACA4415 airfoil lift to drag ratio comparison with Base airfoil and percentage of lift to drag ratio increase

The aerodynamic performance of the various trial cases was compared to the base case, revealing distinct trends.

Trial-1 demonstrated a notable increase in both lift coefficient (Cl) and drag coefficient (Cd), leading to a 20.0% improvement in the lift to drag ratio (Cl/Cd), indicating enhanced aerodynamic efficiency. Similarly, Trial-2 also showed an increase in Cl and Cd, with an 18.1% improvement in the lift to drag ratio. In contrast, Trial-3, despite having a higher Cl than the base case, exhibited a significant rise in Cd, resulting in a 19.0% decrease in the lift to drag ratio, suggesting a decline in aerodynamic performance. Overall, Trials 1 and 2 suggest favorable modifications, while Trials 3 indicates potential drawbacks in aerodynamic efficiency.

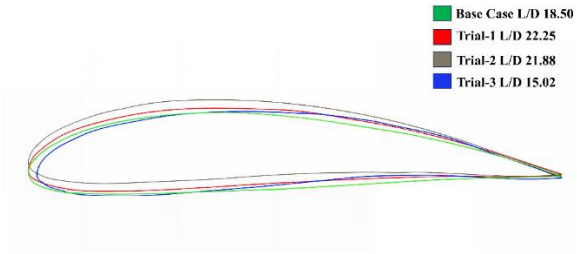

Figure 12: NACA 4415 airfoil shapes compare with Base airfoil after optimization

This figure shows airfoil shape change with lift to drag ratio change. Red marked airfoil is the optimized airfoil compare to all other trials including NACA4415.

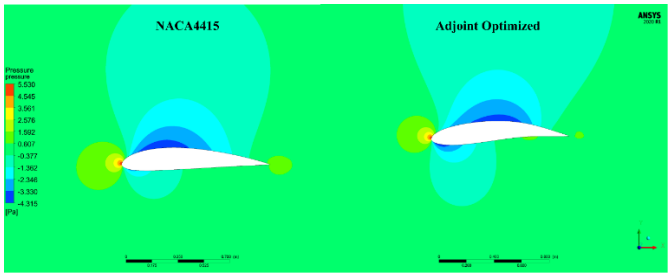

Figure 13: Pressure Contour of NACA4415 and Adjoint optimized airfoil

Figure 13 shows the pressure contour of NACA4415 base airfoil and the adjoint airfoil. Its visible that the low-pressure region above the airfoil increases and creates a comparative high-pressure region at the bottom.

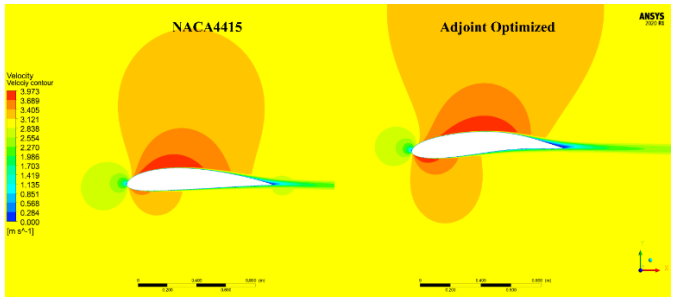

Figure 14: Velocity Contour of NACA4415 and Adjoint optimized airfoil

Velocity contour is depicted in figure 14. On the optimized airfoil, the velocity is quite high on the top compared to the base airfoil. Thus, resulting in low pressure at the top generating a higher lift force.

5. Conclusion

Conducting numerical analysis of NACA4415 with Vortex generator and performed adjoint optimization, these are the summary of the findings:

- Comparing the three vortex generator cases to the base airfoil case reveals distinct performance differences. From Figure 8, VG Case-1 peaks with a lift coefficient (Cl) of 0.9163 at 10 degrees, but its lift to drag ratio drops at higher AOAs. VG Case-2 excels at 5 degrees with a Cl of 0.7258 and a high lift to drag ratio of 25.3260 but collapses at 25 degrees, reaching a low lift to drag ratio of 0.4494. VG Case-3 maintains moderate performance, peaking at 0.8124 at 10 degrees, yet still experiences a decline in efficiency at higher AOAs.
- On adjoint optimization, Trial-1 and Trial-2 show improved aerodynamic efficiency over the base case, while Trial-3 results in reduced performance due to higher drag. Trial-1 showed the best performance, with a 20.23% improvement in the lift to drag ratio, followed by Trial-2 (18.24%). Trial 3 underperformed with an 18.94% reduction, highlighting the need for careful optimization.

References

[1] D. T. Kashid, A. K. Parkhe, S. M. Kale, S. S. Wangikar, C. C. Jadhav, and H. N. Paricharak, "NACA 4415 Aerofoil: Numerical Analysis for Performance in Drag and Lift," *Techno-societal 2022*, pp. 461–474, 2024.

[2] Sudarsono, Purwanto, and J. Wahyuadi, "Optimization Design of Airfoil Propellers of Modified NACA 4415 Using Computational Fluids Dynamics," *Adv. Mater. Res.*, vol. 789, pp. 403–407, 2013.

[3] M. R. Ahmed and S. D. Sharma, "An investigation on the aerodynamics of a symmetrical airfoil in ground effect," *Exp. Therm. Fluid Sci.*, vol. 29, no. 6, pp. 633–647, 2005.

[4] M. Algan, M. Seyhan, and M. Sarioğlu, "Effect of aero-shaped vortex generators on NACA 4415 airfoil," *Ocean Eng.*, vol. 291, p. 116482, Jan. 2024.

[5] M. Z. Akhter and F. K. Omar, "Review of Flow-Control Devices for Wind-Turbine Performance Enhancement," *Energies 2021, Vol. 14, Page 1268*, vol. 14, no. 5, p. 1268, Feb. 2021.

[6] Gad-El-Hak and Mohamed, "Flow Control," *flco*, vol. 17, no. 12, p. 442, 2000, Accessed: Sep. 11, 2024. [Online]. Available: https://ui.adsabs.harvard.edu/abs/2000flco.book.....G/abstract

[7] Z. Zhao *et al.*, "Researches on vortex generators applied to wind turbines: A review," *Ocean Eng.*, vol. 253, p. 111266, Jun. 2022.

[8] A. Arif GÜLER, M. Seyhan, and Y. Erkan AKANSU, "Effect of signal modulation of DBD plasma actuator on flow control around NACA 0015," *J. Therm. Sci. Technol.*, vol. 38, no. 1, pp. 95–105, Apr. 2018, Accessed: Sep. 11, 2024. [Online]. Available: https://dergipark.org.tr/en/pub/isibted/issue/56379/782449

[9] B. Yagiz, O. Kandil, and Y. V. Pehlivanoglu, "Drag minimization using active and passive flow control techniques," *Aerosp. Sci. Technol.*, vol. 17, no. 1, pp. 21–31, Mar. 2012.

[10] R. Çakıroğlu, H. E. Tanürün, A. Acır, F. Üçgül, and S. Olkun, "Optimization of NACA 4412 augmented with a

gurney flap by using grey relational analysis," *J. Brazilian Soc. Mech. Sci. Eng.*, vol. 45, no. 3, pp. 1–18, Mar. 2023.

[11] A. Hövelmann, F. Knoth, and C. Breitsamter, "AVT-183 diamond wing flow field characteristics Part 1: Varying leading-edge roughness and the effects on flow separation onset," *Aerosp. Sci. Technol.*, vol. 57, pp. 18–30, Oct. 2016.

[12] L. Qiao *et al.*, "Improved hybrid model for transitional separated flows over a rough compressor blade," *Aerosp. Sci. Technol.*, vol. 140, p. 108434, Sep. 2023.

[13] Y. Xie, Y. Rao, Y. Cheng, and W. Tian, "Investigation into the laminar separation control of airfoils at low Reynolds numbers by dimple vortex generators," *Aerosp. Sci. Technol.*, vol. 129, p. 107841, Oct. 2022.

[14] W. Chen, W. Qiao, and Z. Wei, "Aerodynamic performance and wake development of airfoils with wavy leading edges," *Aerosp. Sci. Technol.*, vol. 106, p. 106216, Nov. 2020.

[15] C. Papadopoulos, V. Katsiadramis, and K. Yakinthos, "Influence of tubercles' spanwise distribution on swept wings for unmanned aerial vehicles," *https://doi.org/10.1177/0954410020919583*, vol. 235, no. 1, pp. 95–103, Apr. 2020.

[16] E. Sobhani, M. Ghaffari, and M. J. Maghrebi, "Numerical investigation of dimple effects on darrieus vertical axis wind turbine," *Energy*, vol. 133, pp. 231–241, Aug. 2017.

[17] T. K. Zhen, M. Zubair, and K. A. Ahmad, "Experimental and numerical investigation of the effects of passive vortex generators on Aludra UAV performance," *Chinese J. Aeronaut.*, vol. 24, no. 5, pp. 577–583, Oct. 2011.

[18] C. M. Velte, M. O. L. Hansen, K. E. Meyer, and P. Fuglsang, "Evaluation of the Performance of Vortex Generators on the DU 91-W2-250 Profile using Stereoscopic PIV," *Citation*, vol. 2, pp. 263–267, 2008.

[19] B. J. Wendt, "Parametric study of vortices shed from airfoil vortex generators," *AIAA J.*, vol. 42, no. 11, pp. 2185–2195, 2004.

[20] H. Shan, L. Jiang, C. Liu, M. Love, and B. Maines, "Numerical study of passive and active flow separation control over a NACA0012 airfoil," *Comput. Fluids*, vol. 37, no. 8, pp. 975–992, Sep. 2008.

[21] K. P. Angele and B. Muhammad-Klingmann, "The effect of streamwise vortices on the turbulence structure of a separating boundary layer," *Eur. J. Mech. - B/Fluids*, vol. 24, no. 5, pp. 539–554, Sep. 2005.

[22] D. . Bushnell and J. . Hefner, "Viscous Drag Reduction in Boundary Layers," p. 526, 2000, Accessed: Sep. 11, 2024. [Online]. Available: https://books.google.com/books/about/Viscous_Drag_Reduction_in_Boundary_Layer.html?id=8IxMxOwjs8cC

[23] "Turbulent Skin-Friction Drag Reduction By Active and Passive Means. Part 1. Everything you wanted to Know about Riblets, LEBUs and Other Devices,." https://apps.dtic.mil/sti/citations/ADP006971 (accessed Sep. 11, 2024).

[24] P. Vukoslavčević, J. M. Wallace, and J. L. Balint, "Viscous drag reduction using streamwise-aligned riblets," *AIAAJ*, vol. 30, no. 4, pp. 1119–1122, 1992.

[25] X. Cai, D. G. Steyn, and I. S. Gartshorec, *Flow field alteration and viscous drag reduction by riblets in a turbulent boundary layer*. in Near-wall turbulent flows. Elsevier Publishing Company, 1993.

[26] M. Giles, M. Duta, and J.-D. Mueller, "Adjoint code developments using the exact discrete approach," *15th AIAA Comput. Fluid Dyn. Conf.*, 2001, Accessed: Sep. 11, 2024. [Online]. Available: https://www.academia.edu/52284161/Adjoint_code_developments_using_the_exact_discrete_approach

[27] C. S. Kim, C. Kim, and O. H. Rho, "Parallel Computations of High-Lift Airfoil Flows Using Two-Equation Turbulence Models," , vol. 38, no. 8, pp. 1360–1368, May 2012.

[28] E. J. Nielsen and W. K. Anderson, "Recent improvements in aerodynamic design optimization on unstructured meshes," *AIAA J.*, vol. 40, no. 6, pp. 1155–1163, 2002.

[29] M. A. Hoque, M. S. Rahman, K. N. Rimi, A. R. Alif, and M. R. Haque, "Enhancing formula student car performance: Nose shape optimization via adjoint method," Results in Engineering, vol. 20, p. 101636, Dec. 2023.

[30] A. Bueno-Orovio, C. Castro, F. Palacios, and E. Zuazua, "Continuous Adjoint Approach for the Spalart-Allmaras Model in Aerodynamic Optimization," *https://doi.org/10.2514/1.J051307*, vol. 50, no. 3, pp. 631–646, Aug. 2012.

[31] A. Elham and M. J. L. van Tooren, "Discrete adjoint aerodynamic shape optimization using symbolic analysis with OpenFEMflow," *Struct. Multidiscip. Optim.*, vol. 63, no. 5, pp. 2531–2551, May 2021.

[32] J. Brezillon and N. R. Gauger, "2D and 3D aerodynamic shape optimisation using the adjoint approach," *Aerosp. Sci. Technol.*, vol. 8, no. 8, pp. 715–727, 2004.

[33] Tunay, T., Sahin, B., & Ozbolat, V. (2014). Effects of rear slant angles on the flow characteristics of Ahmed body. Experimental Thermal and Fluid Science, 57, 165–176.